Mathematical Modeling of Stray Capacitance for Planar Coil at Megahertz Frequency

Jia-Xiang Song[1, 2, *], Hui-Lin An[1, 2], Yan-Hong Li[2], Chao Zhang[2], and Guo-Qiang Lui[1, 2]

Abstract—The coil stray capacitance is an essential factor for high-frequency coil application, such as wireless power transfer system. In this paper, in order to calculate the planar coil stray capacitance at megahertz frequency, the theory model has been built. Based on the basic capacitance calculation equation, the mathematical model has been deduced carefully. Then, the mathematical model has been evaluated by a series of simulation models. In the simulation part, the error of the variables of the theory model has also been analyzed carefully and quantitatively. In order to verify the theory and simulation model, the verification experiment has been done. The experimental results are consistent with the simulated ones and the theory model. The experimental and simulated results indicate that the theory model of the coil stray capacitance has a satisfactory accuracy, and the model has application potential in the field of wireless power transfer.

1. INTRODUCTION

Inductive power transmission systems are widely used in powering electronic devices such as wireless charging for electric vehicle or sensor networks, radio frequency identification devices, medical implanted devices maglev trains, and many more [1, 2, 6–8].

High efficiency always depends on accurate control, and accurate and fast calculation parameter is essential for accurate control. The most common calculation method of the coil stray capacitance is finite element method (FEM); however, careful calculation of FEM usually has large calculation amount and long computing time [3, 4, 9–11]. Unfortunately, the stray capacitances and resistances are distributed parameters, and the direct measurement of the stray capacitance is difficult. One of the methods measuring the stray capacitance is using the Impedance Analyzer; however, the price of the Impedance Analyzer is expensive. On the other hand, if the measurement result does not satisfy our designing value, the coil will be modified over and over again, and the time and energy will be wasted seriously. Therefore, the theory model of the stray capacitance is very significant for the development of coil system application.

To achieve the accurate and fast calculation of the stray capacitance of a coil system, Massarini and Kazimierczuk [1] derived expressions for calculating the stray capacitance of single and multiple-layer inductors. The equations derived by Massarini and Kazimierczuk are suitable for closely wound coil. However, the air gap between coils was not considered, and in this paper, the problem is considered. In order to estimate self-resonant frequency of Archimedean spiral coils, the stray capacitance is considered in [2], and empirical formulas are also presented. But expect for Archimedean spiral coils, more general coils have not been investigated. Furthermore, the computational efficiency is not high in [2]. In [3], the Finite-Difference Time-Domain method has been applied to calculate the stray parameter. However, this method leads to huge numerical models, and the inhomogeneous surface current distribution is

difficult to solve. In [4], a comprehensive analysis of different methods for the evaluation of L, R_{dc}, and C_s for a coaxial inductor is provided. However, the current methodology may serve to guide the design of optimum coaxial inductors with rectangular cross, and more general cases have not been investigated. In [5], the model is used to predict the self-capacitance of hexagonal winding coils. However, in order to improve the calculation precision, the nonlinear distributed voltage should be considered more carefully.

In this paper, the theory model of the planar coil stray capacitance has been built, and the calculation method can be widely used for coil application. The error of the theory model has been evaluated quantitatively by the simulation models and experience. The rest of the paper is organized as follows. In Section 2, the theoretical analysis of the theory model is deduced in details. In Section 3, the simulation model of the theory model is built, and the variables' influence of the theory model is also analyzed carefully in this part. In Section 4, the verification experiment is done. In Section 5, the conclusion and discussion are presented.

2. METHOD

The planar coil studied in this paper is shown in Figure 1. When the coil inductance needs to couple the capacitance in the coil system, the capacitance is composed of two part: one is the capacitance adding in the electric circuit, and the other is the coil stray capacitance. The influence of stray capacitance will be more forceful when the turn system frequency increases. Thus, in this paper, the model of coil stray capacitance is built taking an example of planar coils, and the calculation method can be widely used for the coil system.
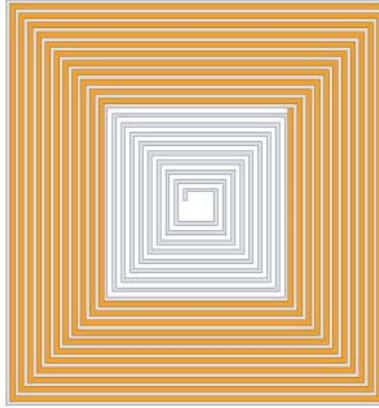
Figure 1. Diagram of planar coil studied in this paper.

The total stray capacitance consists of the following components:
1) Capacitance of the Insulating Layer of Coils;
2) Capacitance of the Gap Filled with Supporting Part.

The cross-sectional view of planar coils is shown in Figure 2. The unit of stray capacitance includes four basic cells, and the four basic cells ABCD of the turn-to-turn capacitance unit are shown in Figure 3. We assume that the capacitance of basic cell A is equal to basic cell C due to the symmetry of geometry. For simplicity, we assume that the capacitance of basic cell B is equal to basic cell D because they are both small.
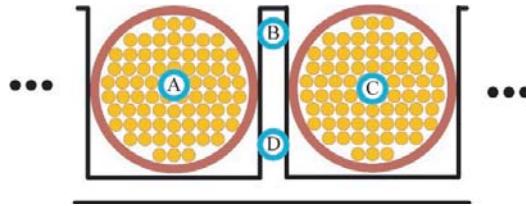
As the coil is made by Litz wire, the diameter of single turn of Litz wire is 0.01 mm; the radius of single turn of Litz wire is 5×10^{-2} mm; the skin depth of the coil is

$$\Delta d = \sqrt{\frac{2}{\omega \mu \sigma}} \tag{1}$$

where Δd is the skin depth of the coil, ω the system angular frequency ($\omega = 2\pi f$, f is the system frequency), μ the permeability, and σ the conductivity of the material.
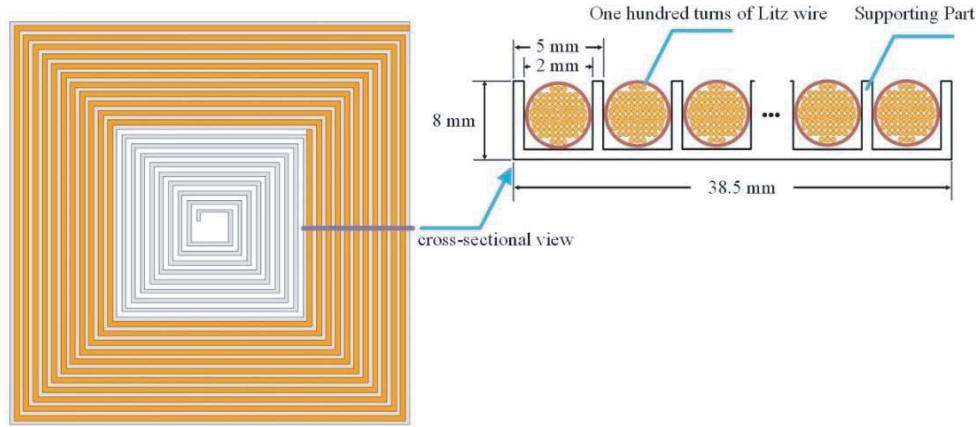
Figure 2. The cross-sectional view of planar coils in this paper.

Figure 3. The basic cell ABCD related to the turn-to-turn capacitance.

In this paper, the system frequency ω is assumed $1\,\text{MHz}$; the material of Litz wire is copper ($\sigma = 5.8 \times 10^7\,\text{S/m}$, $\mu = 4\pi \times 10^{-7}\,\text{H/m}$); the skin depth of the coil Δd is $6.62 \times 10^{-2}\,\text{mm}$; and Δd is greater than the radius of single turn of Litz wire, thus the skin effect is tiny. Therefore in this paper, the skin effect of the coil is not considered. If we consider two adjacent conductors, the elementary capacitance dS between two opposite corresponding elementary surfaces of these conductors Δd is given by

$$dC = \varepsilon \frac{dS}{x} \qquad (2)$$

where $\varepsilon = \varepsilon_0 \varepsilon_r$ is the permittivity of the medium, and x is the length of a line of the electric field connecting the two opposite elementary surfaces. In the most general case, length x is not constant, but length x can be a function of the location of the elementary surface. In this paper, a round conductor is selected, and the location of each elementary surface can be described by one angular coordinate θ, shown in Figure 4 and Figure 6. The elementary capacitance dC also depends on the angular coordinate θ.

2.1. Method of Turn-to-Turn Capacitance

In Figure 4, the lines of the electric field are cross three different regions: two insulating layers of two turns, the air gap between two turn, and the air gap filled with the supporting part. Therefore, the elementary capacitance dC is equivalent to the series connection capacitance of three different regions elementary capacitances: the first capacitor is the insulating layer of the first turn; the second capacitor is the air gap capacitance; and the third capacitor is the insulating layer of the second turn.

2.1.1. Capacitance of the Insulating Layer

In this part, the expression of the insulating layers capacitance will be derived. An elementary cylindrical surface located between the conductor surface and external insulating layer surface is shown in Figure 5.
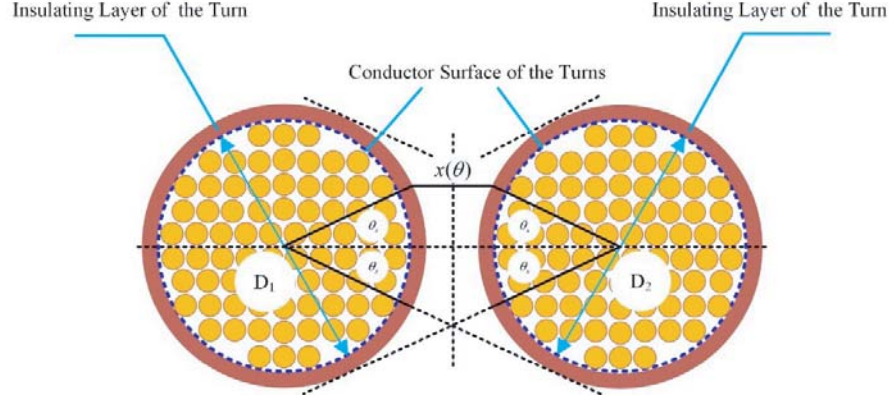
Figure 4. Diagram of each elementary surface can be described by one angular coordinate.
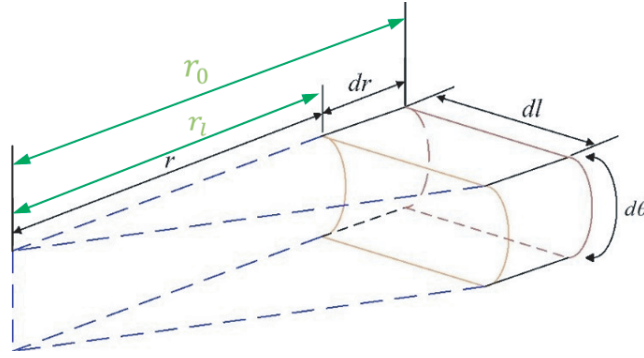
Figure 5. Diagram of the capacitance between the conductor surface and external layer surface.

The elementary capacitance of the cylindrical layer shell is given by

$$dC = \frac{\varepsilon_r \varepsilon_0 r}{dr} d\theta dl \tag{3}$$

where ε_r is the relative permittivity of the dielectric, and ε_0 is the dielectric constant of vacuum.

With integral r in Equation (3) from the radius of conductor r_l to the outer radius of wire r_0 and integral l from zero to the turn length l_t, the insulating layer capacitance will be obtained:

$$dC_l = \varepsilon_r \varepsilon_0 d\theta \int_0^{l_t} dl \int_{r_l}^{r_0} \frac{r}{dr} = \int_0^{l_t} \frac{\varepsilon_r \varepsilon_0}{\ln \frac{r_0}{r_l}} dl d\theta \tag{4}$$

Therefore, the capacitance per unit angle of the insulating layer is given by

$$\frac{dC_{ttl}}{d\theta} = \frac{dC_l}{2} = \int_0^{l_t} \frac{\varepsilon_r \varepsilon_0}{2 \ln \frac{r_0}{r_l}} dl \tag{5}$$
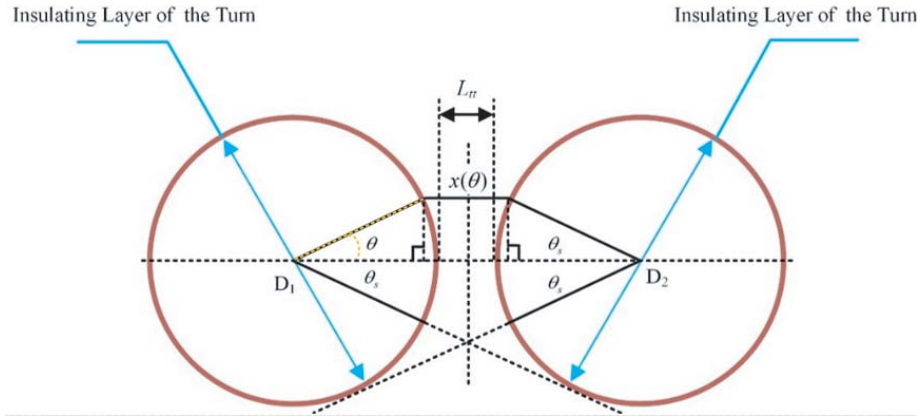
2.2. Capacitance of the Air Gap Filled with Supporting Part

In Figure 6, θ is a variable; the minimum value of θ is 0; the maximum value of θ is θ_s; the θ is the angle of coil center wire with a line of the electric field as shown in Figure 6. The length of the assumed paths $x(\theta)$ is a function of θ:

$$x(\theta) = L_{tt} + \frac{(D_1 + D_2)(1 - \cos\theta)}{2} \tag{6}$$

In this paper, the diameter of the coil turn is equal to

$$D_0 = D_1 = D_2 \tag{7}$$

Figure 6. Geometrical relationship of capacitance of the air gap filled with supporting part.

Thus, the length of the assumed paths is

$$x(\theta) = L_{tt} + D_0 (1 - \cos\theta) \tag{8}$$

Assume that the length of the elementary turn is l_t, and the elementary surface of the wire is

$$dS = \frac{l_t D_0}{2} d\theta \tag{9}$$

As $dC = \varepsilon \frac{dS}{x}$, the elementary capacitance of air gap is

$$dC_{ag} = \varepsilon_0 \varepsilon_r \frac{l_t D_0}{2 x(\theta)} d\theta \tag{10}$$

Combining with Equation (6), the air gap elementary capacitance is

$$dC_{ag} = \varepsilon_0 \varepsilon_r \frac{l_t D_0}{2 [L_{tt} + D_0 (1 - \cos\theta)]} d\theta \tag{11}$$

The per unit angle of the air gap elementary capacitance is

$$\frac{dC_{ag}}{d\theta} = \varepsilon_0 \varepsilon_r \frac{l_t D_0}{2 [L_{tt} + D_0 (1 - \cos\theta)]} \tag{12}$$

Thus, the air gap capacitance is

$$C_{ag} = \varepsilon_0 \varepsilon_r D_0 l_t \frac{\arctan\left[\dfrac{\tan\left(\dfrac{\theta}{2}\right)(4D_0 + 2L_{tt})}{\sqrt{2\left(L_{tt}^2 + 2D_0 L_{tt}\right)}}\right]}{\sqrt{L_{tt}^2 + 2D_0 L_{tt}}} \tag{13}$$

2.2.1. Total Turn-to-Turn Basic Cell Capacitance

The series combination of the elementary capacitances in Equation (5) and Equation (12) is given by

$$dC_{eq}(\theta) = \frac{dC_{ttl} dC_{ag}}{dC_{ttl} + dC_{ag}} \tag{14}$$

Combining with Equation (6) and Equation (12), Equation (13) is

$$dC_{eq}(\theta) = \varepsilon \varepsilon_r \frac{\dfrac{l_t D_0}{2 [L_{tt} + D_0 (1 - \cos\theta)]} \displaystyle\int_0^{l_t} \dfrac{1}{\ln D_0 - \ln D_1} dl}{\displaystyle\int_0^{l_t} \dfrac{1}{\ln D_0 - \ln D_1} dl + \dfrac{l_t D_0}{L_{tt} + D_0 (1 - \cos\theta)}} d\theta \tag{15}$$

With integral θ in Equation (15), the overall turn-to-turn basic cell capacitance is

$$C_{tt} = \int_0^{\theta_s} \varepsilon\varepsilon_r \frac{\dfrac{l_t D_0}{2\left[L_{tt} + D_0\left(1 - \cos\theta\right)\right]} \displaystyle\int_0^{l_t} \dfrac{1}{\ln D_0 - \ln D_1}dl}{\displaystyle\int_0^{l_t} \dfrac{1}{\ln D_0 - \ln D_1}dl + \dfrac{l_t D_0}{L_{tt} + D_0\left(1 - \cos\theta\right)}}d\theta \tag{16}$$

2.3. Overall Stray Capacitance of the Single Layer Coil

In this part, the case of unequal turn ($n \geq 2$) model will be built. For a single-layer coil consisting of n turns, the overall stray capacitance of the coil can be calculated by the lumped capacitor network.

Firstly, in the case of $n = 2$, the electric field lines cross the air gap between the two turns. The material between the two turns is assumed all supporting part (dielectric constant is 2.5). The diagram of the case of single-layer with two turns is shown in Figure 7.
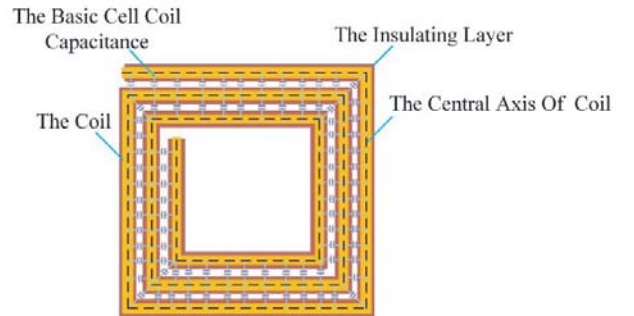
From Equation (15), dC_{eq} is a function about insulating layer angle θ and integral the angle θ, then the expression of the overall stray capacitance of two turns will be obtained:

$$C_{overall} = 2\varepsilon_0\varepsilon_r D_0 l_t \frac{act\left(\dfrac{\tan\left(\dfrac{\theta}{2}\right)\left(8D_0 + 4L_{tt} + 2D_0\ln\dfrac{D_0}{D_l}\right)}{\sqrt{2\left(D_0^2\ln\left(\dfrac{D_0}{D_l}\right)^2 + 4D_0^2\ln\dfrac{D_0}{D_l} + 4D_0 L_{tt}\ln\dfrac{D_0}{D_l}\right) + 8D_0 L_{tt} + 4L_{tt}^2}}\right)}{\sqrt{D_0^2\ln\left(\dfrac{D_0}{D_l}\right)^2 + 4D_0^2\ln\dfrac{D_0}{D_l} + 8D_0 L_{tt} + 4L_{tt}^2}} \tag{17}$$

Secondly, we consider the case of $n = 3$, and the network consists of the capacitance between turns 1, 2, and 3. The material between turns is assumed supporting part (dielectric constant is 2.5). Diagram of the case of three turns is shown in Figure 8.
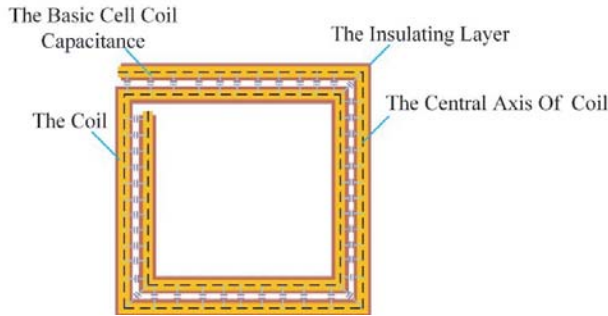
Figure 7. Diagram of the case of single-layer with two turns.

Figure 8. Diagram of the case of single-layer with three turns.

From Equation (15), dC_{eq} in the case of $n = 3$ is also a function about angle θ. Compared with the case of $n = 2$, the case of three turns has two air gaps, and the two air gap capacitance is series connection. Moreover, the value of the air gap capacitance will be decreased with the number of coil turns increasing. The relationship between the different numbers of coil turns can be described simplistically:

$$C_{airgap.n} = \frac{C_{airgap.n-1}}{n-1} \tag{18}$$

Here, $C_{airgap.n}$ is the air gap capacitance in the case of n coil turns, and $C_{airgap.n-1}$ is the air gap capacitance in the case of $n - 1$ turns. The calculation method of the case of $n \geq 3$ is the same as the case of $n = 3$.

Thus, in this part, the model of calculating the case of unequal turns is built. The method of the air gap capacitance is different between the case of $n = 2$ and the case of $n \geq 3$.

3. NUMERICAL SIMULATION BY THE FINITE ELEMENT METHOD

In this part, the finite element method (FEM) is used to test and verify the theory model which is presented in the second part.

3.1. Simulation of the Insulating Layer Capacitance

The insulating layer capacitance simulation model is built, as shown in Figure 9.
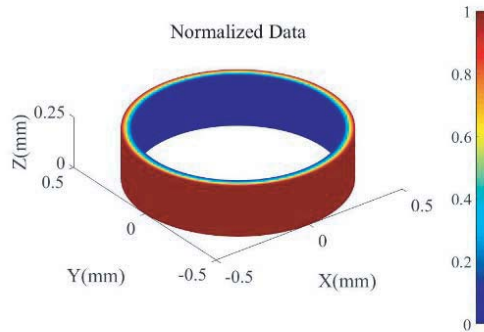
Figure 9. Diagram of the simulation model of capacitance of the insulating layer.

The theory results are solved based on Equation (4), and compared with the simulation ones. We change the parameters of the geometric model, such as the coil length l_t, the thickness of insulating layer d_r, the radius of the turn r_l, and the integral angle θ. We calculate the simulation capacitance C_{ls} for every different parameter of the geometric model, as shown in Figure 10.

Based on control variable method, in Figure 10, we can find that the expression of the coil length l_t is accurate in the theory model, and the expression of the thickness of insulating layer d_r is also accurate in the theory model.

In Figure 10(c), the difference between the theory and simulation results will expand with the value of r_l increasing, and this phenomenon may be caused by the end effect of the model. In this paper, the radius of the turn r_l is 0.5 mm, and the error of the theory model is acceptable. In Figure 10(d), the theory results are a little different from the simulation, because the end effect is not considered in the theory model. In practice, the integral angle of the insulating layer is almost equal to π, thus the error between the theory and simulation is tiny.

3.2. Simulation of the Air Gap Capacitance

Based on Figure 6, the air gap capacitance simulation model is built, and the diagram is shown in Figure 11.

In Figure 11(a), electric field wires are mainly concentrated between the two coil wires. In Figure 11(b), the area with high electric field strength is between two wires, which is consistent with the hypothesis in the theoretical model.

In order to test and verify the theory model of the air gap capacitance, we solve the theory results of air gap capacitance based on Equation (13), and compare them with the simulation results. We change the parameters of the geometric model in Figure 6, such as the coil length l_t, the diameter of turn D_0, the distance between the coils L_{tt}, and the angle of electric field line θ shown in Figure 6.

In Figures 12(a) and (b), we can find that the expression of the coil length l_t is accurate in the theory model, and the expression of the distance between two turns L_{tt} is also accurate in the theory
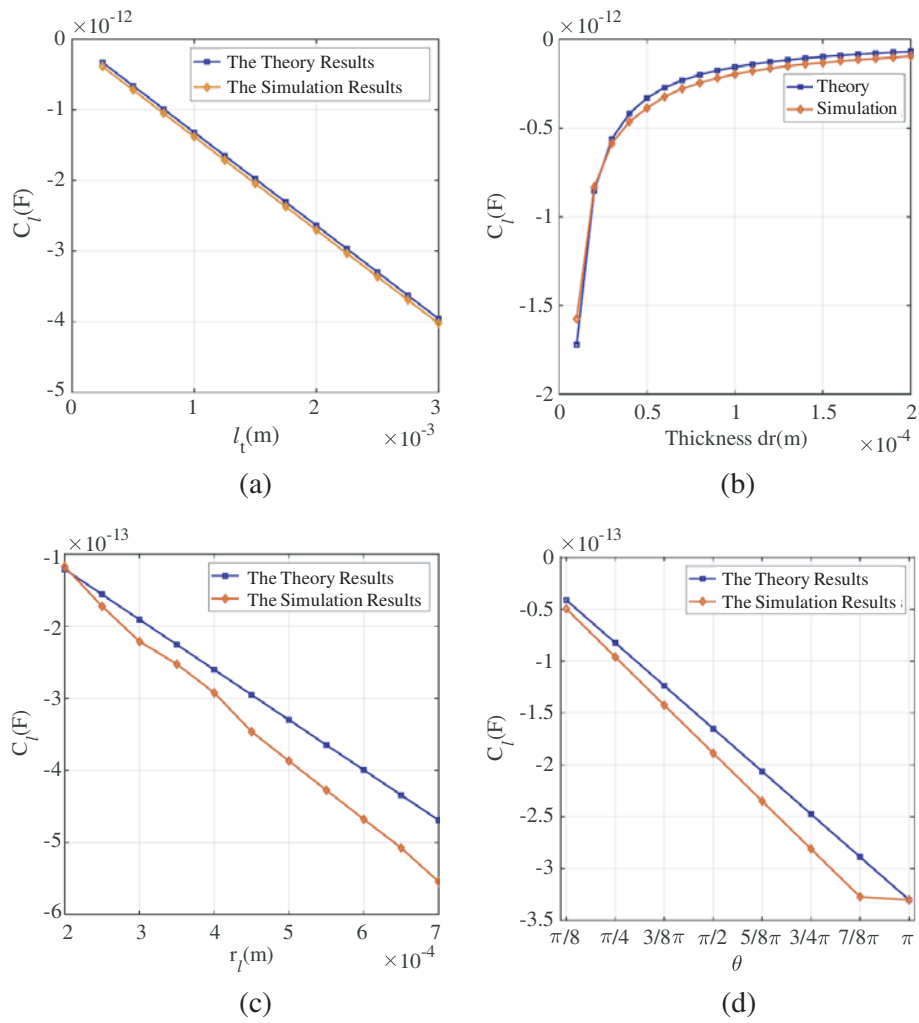
Figure 10. Diagram of the capacitance of the insulating layer calculated by the theory and FEM.
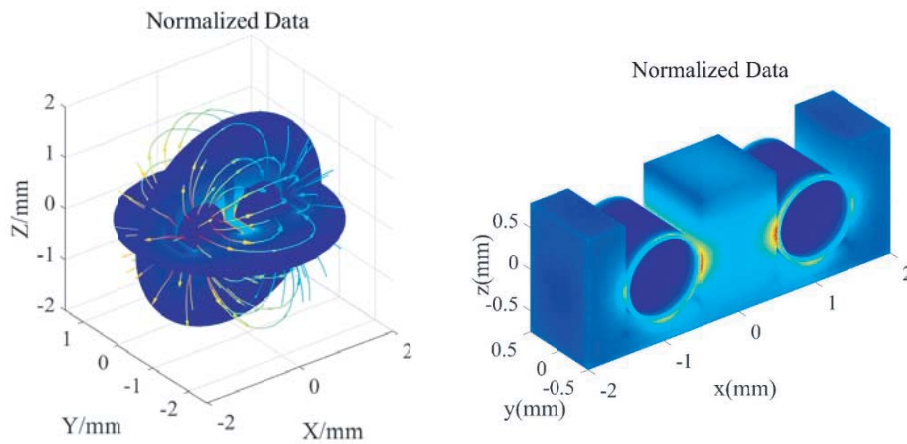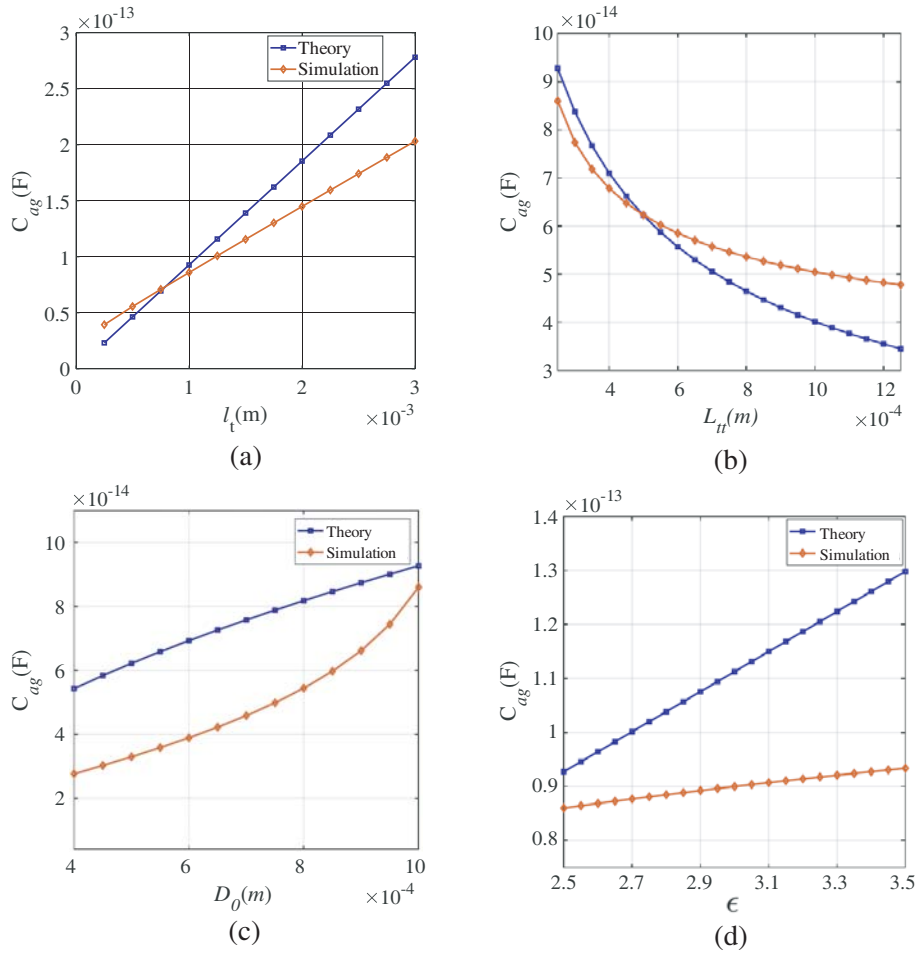

Figure 11. Diagram of simulation model of the air gap capacitance filled with supporting part.

Figure 12. The Capacitance of the Air Gap calculated by the theory and FEM.

model. However, there is also difference between the simulation and theory model. The difference may be caused by the end effect, and the theory model does not consider the end effect.

In Figure 12(c), the difference is tiny when the diameter D_0 of two turns is $1\,\text{mm}$, and in most cases of coil system, the diameter of turns of coil is about $1\,\text{mm}$ or exceed $1\,\text{mm}$. Thus, the difference between the theory and simulation results is acceptable.

In Figure 12(d), comparing the theory results with the simulation ones, the difference can be found. The reason for the difference is: the air gap is filled with the supporting part, but the air is also around the supporting part; for simplicity, in the theory model, the dielectric constant of the background is all assumed ε_r, and in the finite element method model the region of the supporting part and the air is built as practical situation. Thus, in practice, the turn should be embedded in the supporting part.

4. A VERIFICATION EXPERIMENT

A verification experiment coil has been designed to evaluate the proposed mathematical model. A 3D verification simulation model is also built with the same size of experiment coil. The experiment results are compared with simulation ones, which verifies the proposed mathematical model.
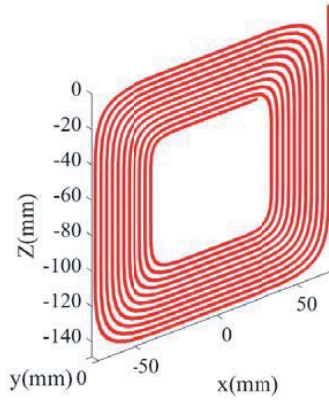
4.1. 3D Verification Experiment

The parameters of 3D verification simulation model are shown in Table 1, and the diagram of the simulation model of 3D verification simulation model is shown in Figure 13. Calculating the total stray

Table 1. The parameters of 3D verification simulation model.

Parameter	L_{tt}	D_0	D_l	θ_s
Value	$2\,\text{mm}$	$0.8\,\text{mm}$	$0.7\,\text{mm}$	2π

capacitance of the simulation coil by using the FEM in COMSOL Multiphysics [17–19], electrostatic module is chosen as the solution module of software; the potential difference of the model is 1 V; and the material of supporting part in the simulation model is assumed as insulation material whose dielectric constant is 2.5. The simulation coil is designed in the same plane (yz-plane) as shown in Figure 13.

Figure 13. Diagram of the simulation model of 3D verification simulation model.

4.2. Experiment

With the verification simulation settings, the experiment is done. The picture of experiment coil is shown in Figure 14. The experiment coil is measured by Impedance Analyzer. The name of the Impedance Analyzer is Keysight Technology, and the model of the Impedance Analyzer is e4990a. To avoid the measurement error, the experiment coil has been measured three times, and the final measurement result of stray capacitance is the average of the three measurement results [20, 21].

Figure 14. The picture of experiment coil.

4.3. Comparison between the Results of Verification and Experiment

Stray capacitances are $8.01\,\mathrm{pF}$ and $6.66\,\mathrm{pF}$ in simulated and experimental results, respectively. The difference between experiment and simulation results is:

$$\Delta e = \frac{|C_E - C_s|}{C_s} \times 100\% = \frac{|6.66 - 8.01|}{8.01} \times 100\% = 16.85\%$$

Here, Δe is the error of the experiment measurement result and the simulation result, C_E the experiment measurement result, and C_s the simulation result.

The difference is calculated, $\Delta e = 16.85\%$, and the value of Δe is lower than most of the references [1–4, 12–16]. Thus, the experimental result is consistent with the simulated one, and the mathematical model has been verified.

5. CONCLUSION

In this paper, the theory model of stray capacitance for Planar Coil at Megahertz Frequency has been built. The error of the theory model has been evaluated by the simulation models precisely and quantitatively. Moreover, on the same condition, the simulation results are very close to the theory ones, and the error is 16.85%. The verification experiment has also been done, and Δe is used for evaluating the difference of the simulation results with the experiment results quantitatively. Δe is 16.85% lower than most references, which will help design the wireless power transfer system more precisely. Thus, the experiment and simulation results indicate that the calculation model can improve the calculation accuracy of the coil stray capacitance.

It is worthy to note that the error between the theory and simulation results will increase with increasing wire diameter, because we assume that the paths of the electric field in the air gap are the shortest possible paths; the assumption is a conservative approximation. The accuracy of the assumption will be worse when the wire diameter increases, thus the theory model can be applied to the thin wire. At present, the theory model is verified to apply to the case of the diameter of wire less than $2\,\mathrm{mm}$. However, in a coil system, a thin wire is widely used to avoid the skin effect, and serious skin effect will decrease the efficiency of a coil system. Moreover, the simulation results also have some difference from the experiment results, and lower Δe will be more conducive to improving the efficiency of coil system, thus a more careful theory model is still needed. Finally, the final calculation equation is a complex equation, and the equation could be simplified in some cases which will be more suitable for engineering application. These problems are not included in this paper, and the improvements will be studied in future research.

REFERENCES

1. Massarini, A. and M. K. Kazimierczuk, "Self-capacitance of inductors," *IEEE Transactions on Power Electronics*, Vol. 12, No. 1, 33–40, 1997.
2. Yun, H. C., G. Lee, and W. S. Park, "Empirical formulas for self-resonance frequency of Archimedean spiral coils and helical coils," *Proceedings of the 2012 IEEE International Symposium on Antennas and Propagation*, 1–2, 2012.
3. Sijoy, C. D. and S. Chaturvedi, "Calculation of accurate resistance and inductance for complex magnetic coils using the finite-difference time-domain technique for electromagnetics," *IEEE Transactions on Plasma Science*, Vol. 36, No. 1, 70–79, 2008.
4. Martinez, J. L., S. Babic, and C. Akyel, "On evaluation of inductance, dc resistance, and capacitance of coaxial inductors at low frequencies," *IEEE Transactions on Magnetics*, Vol. 50, No. 7, 1–12, 2014.
5. Rizzoli, G., M. Mengoni, A. Tani, G. Serra, and D. Casadei, "Wireless power transfer using a five-phase wound-rotor induction machine for speed-controlled rotary platforms," *IEEE Transactions on Industrial Electronics*, Vol. 67, No. 8, 6237–6247, 2020.
6. Kurs, A., A. Karalis, R. Moffatt, J. D. Joannopoulos, P. Fisher, and M. Soljacic, "Wireless power transfer via strongly coupled magnetic resonances," *Science*, Vol. 317, No. 5834, 83–86, 2007.

7. Beeby, S. P., M. J. Tudor, and N. M. White, "Energy harvesting vibration sources for microsystems applications," *Measurement Science & Technology*, Vol. 17, No. 12, 175–195, 2006.

8. Li, S. and C. C. Mi, "Wireless power transfer for electric vehicle applications," *IEEE Journal of Emerging and Selected Topics in Power Electronics*, Vol. 3, No. 1, 4–17, 2015.

9. Yao, R., et al., "A combined system for generating a uniform magnetic field and its application in the investigation of Efimov physics," *Chinese Physics B*, Vol. 27, No. 1, 16703-016703, 2018.

10. Xu, Z., et al., "Equivalent magnetic dipole method used to design gradient coil for unilateral magnetic resonance imaging," *Chinese Physics B*, Vol. 27, No. 5, 058702, 2018.

11. Lu, W.-G., et al., "Numerical analysis of magnetic-shielding effectiveness for magnetic resonant wireless power transfer system," *Chinese Physics Letters*, Vol. 34, No. 08, 155–158, 2017.

12. Ezheiyan, M., et al., "Thermal analysis simulation of germanium zone refining process assuming a constant radio-frequency heating source," *Chinese Physics Letters*, Vol. 33, No. 5, 123–126, 2016.

13. Li, S., "New discrete element models for three-dimensional impact problems," *Chinese Physics Letters*, Vol. 26, No. 12, 5–8, 2009.

14. Kellnberger, S., A. Rosenthal, A. Myklatun, G. G. Westmeyer, G. Sergiadis, and V. Ntziachristos, "Magnetoacoustic sensing of magnetic nanoparticles," *Physical Review Letters*, Vol. 116, No. 10, 108103.1–108103.6, 2016.

15. Pillsbury, R. and W. Punchard, "A finite element/fourier expansion technique for the design of a pulsed radial gradient system for magnetic resonance imaging (MRI)," *IEEE Transactions on Magnetics*, Vol. 21, No. 6, 2273–2275, 1985.

16. Zhang, Z. and B. Zhang, "Angular-misalignment insensitive omnidirectional wireless power transfer," *IEEE Transactions on Industrial Electronics*, Vol. 67, No. 4, 2755–2764, 2020.

17. Lin, D., C. Zhang, and S. Y. R. Hui, "Mathematic analysis of omnidirectional wireless power transfer — Part-II three-dimensional systems," *IEEE Transactions on Power Electronics*, Vol. 32, No. 1, 613–624, 2017.

18. Kim, Y. G. and S. Nam, "Determination of the impedance parameters of antennas and the maximum power transfer efficiency of wireless power transfer," *IEEE Transactions on Antennas and Propagation*, Vol. 67, No. 8, 5132–5144, 2019.

19. Minnaert, B. and N. Stevens, "Conjugate image theory applied on capacitive wireless power transfer," *Energies*, Vol. 10, No. 1, 46, 2017.

20. Lu, H. Y., J. G. Zhu, and S. R. Y. Hui, "Experimental determination of stray capacitances in high frequency transformers," *IEEE Transactions on Power Electronics*, Vol. 15, No. 8, 1105–1112, 2003.

21. Riba, J. R., F. Capelli, and M. Moreno-Eguilaz, "Analysis and mitigation of stray capacitance effects in resistive high-voltage dividers," *Energies*, Vol. 12, No. 12, 2278, 2019.